UNIVERSAL WISER
PUBLISHER

Monte Carlo Approach Towards Evaluating Random Number Generators Based on Mathematical Schemes Driven from Chua's Circuit

Kasra Amini[1,2*], Aidin Momtaz[3], Ehsan Qoreishi[3], Sarah Amini[4], Sanaz Haddadian[5]
[1]Faculty of Mechanical Engineering, RWTH Aachen University, Aachen, Germany
[2]Institute of Aircraft Propulsion Systems, University of Stuttgart, Stuttgart, Germany
[3]Department of Physics, Isfahan University of Technology, Isfahan, Iran
[4]Department of Computer Engineering, K. N. Toosi University of Technology, Tehran, Iran
[5]System and Circuit Technology Group, Heinz Nixdorf Institute, University of Paderborn, Paderborn, Germany
Email: kasra.amini@rwth-aachen.de

Abstract: The philosophical nature of randomly generated quantities is widely discussed in the realms of chaos theory. Although, the fundamental premise of the chaos theory does not assume any random behavior in the resulting series and considers them deterministic however highly dependent on the initial conditions of the system, one could address the problem of randomness, by using the output of a chaotic system, as the input of a mathematical function, aiming for the generation of randomly distributed values. For that matter, the voltages of the two capacitors in the classic configuration of a Chua's circuit have been measured. Having defined eight mathematical schemes for manipulating the inputted data set, the current manuscript focuses on the pragmatic and engineering criteria of the resulting data, in terms of randomness, and spectral distributions; hence proposing methods of random data generation. The ranking of schemes has been proceeded through a geometrical manifestation of the Monte Carlo Integration. And the suggested eight schemes are compared with the commercially common timer-based random generators. As the geometrical domain in the Monte Carlo Integration has defined in such a way that the most randomly distributed data set would result in a closer estimation of the number Pi, the suggested scheme working based on 'frequency indicator' is evaluated as the highest-ranked scheme in that regard, with the estimated numerical value of 3.1424 for Pi.

***Keywords*:** chaos theory, chaotic circuits, Chua's circuit, Monte Carlo Integration algorithm, randomness

Nomenclature

B_P	Breakpoint of current through Chua's diode
C_1	Capacitor no. 1
C_2	Capacitor no. 2
G_a	Inner slope of Chua's diode
G_b	Outer slope of Chua's diode
i_L	Inductor current
i_R	Chua's diode current
L	Self-inductance
R	Resistance
V_{C_1}	Voltage of Capacitor no. 1
V_{C_2}	Voltage of Capacitor no. 2
V_R	Voltage of Chua's diode
V_{11}	Voltage of Capacitor no. 1 in first experiment
V_{12}	Voltage of Capacitor no. 1 in second experiment
V_{21}	Voltage of Capacitor no. 2 in first experiment
V_{22}	Voltage of Capacitor no. 2 in second experiment
T	Time interval
x	Inputs extracted from capacitor no. 1
y	Inputs extracted from capacitor no. 2
U	Unit Step Function

DOI: https://doi.org/10.37256/cm.142020491

1. Introduction

Chaos theory, the science of nonlinear topics, has lots of applications in engineering, physics, economics, etc. Although it fails to predict the precise condition of the system in different topics such as weather forecast, demographic patterns in biology, three-body problem, etc. However, in the current study this feature has been used to make progress in various fields such as private communications[1-2].

Lorenz derived a three-dimensional system from a drastically simplified model of convective flows in the atmosphere. He found out that the solution of some systems has oscillating irregularities, which cause the outputs not to have a repetitive pattern, however they could be limited in a bounded region of phase space. He discovered the trajectories settled onto a complicated set, while plotting them in three dimensions. This complicated set is called a "strange attractor". The strange attractor is a fractal, unlike fixed points and limited cycles, with a fractional dimension between 2 and 3[3].

Chaos is a fundamental property that possesses nonlinearity and sensitive dependence on initial conditions. It is associated with the complex and unpredictable behavior of phenomena over time, which means being inputs on the series initial condition, the value of the series at any time is a specified nonlinear function of the previous values. Any alteration of the initial conditions makes it impossible to determine the outcome of the system with the desired prediction accuracy[4]. Hence the nonlinearity of a chaotic system makes it display highly erratic and chaotic behavior over a given time interval[5-6]. This feature made chaos undesirable and it was strongly avoided in research[5, 7-9]. But recent breakthroughs have found some new procedures for chaos, where it is intentionally created for unconventional applications; for example, in the field of secure communication[2, 9, 10]. Therefore, there has been a growing interest in exploring systems displaying unusual and complicated waveforms[11].

Chua's circuit could be considered as an example of how chaos theory affects the accuracy of predictions over a given time interval. Therefore, in the last decade, it has been used as a prototype of studying dynamics and control algorithms of nonlinear circuits[7]. Several investigations on Chua's circuit have been developed to find its different applications and enhancing the accuracy of output tracking or validating particular theories such as bifurcation and synchronization[12]. Chaotic circuits have widely absorbed the attention due to their applications in chaos control[13], signal encryption[14], test platform for synchronization and private communications[1, 15]. In addition, the easy implementation of these circuits has made it possible to study chaos in the electronics background. Chaotic features of electronic circuitry, especially in the frame of chaotic attractors have made them beneficial to be used in some practical problems such as genetic algorithms, which are inspired by Darwin's theory of natural selection, to improve its optimization capacities[16-18].

Chaotic circuits could also be used as random number generators in cryptography and particularly Chua's circuit is used as a pseudo random sequence generator[16]. A new chaotic cryptosystem is presented in [19], which also deals with few problems appearing in cryptosystems.

Chua's circuit plays an important role in chaos communications. In order to enhance the level of security in such systems, different techniques have been investigated, such as chaotic masking, chaotic switching and chaotic modulation. These approaches to private communications are based on the combination of synchronization and unpredictability of chaos using Chua's circuit or an analog circuit implementation of the Lorenz system[1]. Comparing the methods in output tracking for having the best results is a necessity in chaotic communications. Reducing the tracking error in the presence of a deterministic disturbance due to coupled circuits and having those signal sources work together in close proximity are examples of the difficulties in this field[12, 20-24].

Bifurcation and chaotic phenomena could be observed in many nonlinear electronic circuitry[25]. Chua's circuit is the most significant setup, since it is the simplest electronic circuit to produce chaotic data, whereas dynamically the most complex among nonlinear circuits yet. In addition, it is the only system, in which the presence of chaos has been mathematically proven[26-30]. These characteristics have made Chua's circuit a standard sample for studying chaotic phenomena[22]. It has been shown that dynamic behavior of Chua's circuit is extended using fractional derivative by non-local and non-singular kernel by the means of numerical analysis for the solution[28].

Monte Carlo methods are defined as a class of computational algorithms, that could be applied to a considerable range of problems. The important role of Monte Carlo methods in statistical physics and their influence in later high technical algorithms to quantify systematic and statistical errors are undeniable. Demonstrating a solution to a problem as a parameter, that is going to be estimated by sampling a given distribution of data is the main idea behind the Monte Carlo algorithm. The general goal of Monte Carlo methods is to approximately provide analytical or numerical solutions, where they are too challenging for implementation. The algorithm will perform a deterministic calculation with possible inputs and analyze the results statistically. In the current research, the attention will be on Monte Carlo Integration, which is the most common application of the mentioned method. The core idea behind the Monte Carlo Integration algorithm is to compensate for

lack of precise information on the boundaries and geometric definitions of the problem set, with a higher than necessary sweeping the domain with randomly generated sets and evaluating the problem thereafter. This higher number of random sets, and the fact that based on the initial premises of the Monte Carlo algorithm, and the experiment should be performed more than a certain threshold limit, causes a numerically over-saturation leading to an approximate value[31].

Finally, it is worth mentioning, that the current manuscript addresses the output signal of an experimental Chua's circuit in its core classical configuration, and the degree of randomness corresponding to it. First, the output signal is mathematically manipulated in certain ways to generate several desired sets of so-called random data, which are extracted from the Chua's circuit experimentally. Then the interpreted data are inputted to the Monte Carlo Integration algorithm in order to evaluate the results and allocate the level of randomness to each individual case.

2. Chua's circuit

2.1 Circuit architecture

The classical Chua's circuit first presented by L. O. Chua and his colleagues in 1984[32], is a nonlinear oscillator, which consists of four linear elements being an inductor, a resistor and two capacitors, as well as a nonlinear element, which could provide an active negative resistance (N_R) called Chua's diode. Chua's diode is not a commercially available device, however, there are various circuit solutions to synthesize N_R using the standard active and passive elements available in the market, mostly including an operational amplifier (op-amp) as the active device[33].

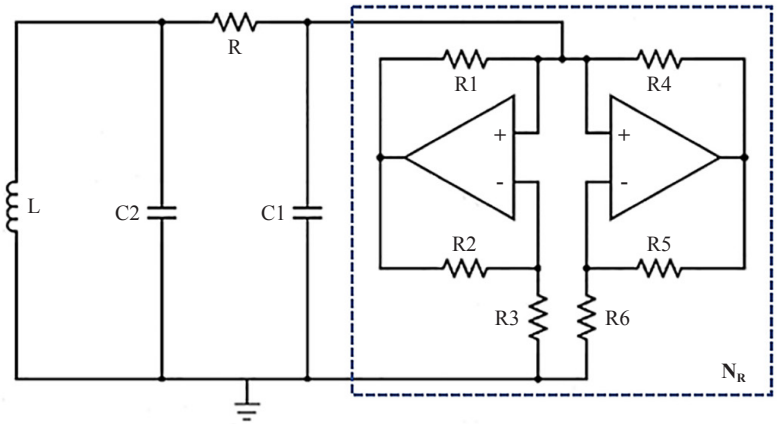

Figure 1. Classical configuration of Chua's circuit

Figure 1 represents the classical Chua's circuit with the Chua's diode implemented using a combination of resistors R1 to R6 and operational amplifiers. Another common alternative solution for the implementation of Chua's diode is shown in Figure 2, consisting of an operational amplifier and PN-junction diodes[34].

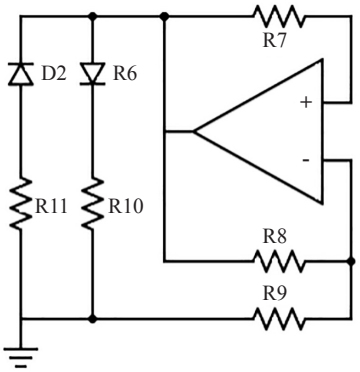

Figure 2. Diode included configuration of Chua's diode (N_R)

2.2 Governing equations

The dynamics of Chua's circuit could be modeled by the following set of nonlinear ordinary differential equations[25].

$$C_1 \frac{dV_R}{dt} = \frac{V_{C_2} - V_R}{R} - f(V_R) \tag{1}$$

$$C_2 \frac{dV_{C_2}}{dt} = iL - \frac{V_{C_2} - V_R}{R} \tag{2}$$

$$L \frac{di_L}{dt} = -V_{C_2} \tag{3}$$

Where, V_{C_1}, V_{C_2} and i_3 denote the voltages of the capacitors C_1 and C_2 and the current of the inductor L, respectively, and $f(V_R)$ is a nonlinear function defined as;

$$i_R = f(V_R) = G_b V_R + \frac{(G_a - G_b) \times \{|V_R + B_P| - |V_R - B_P|\}}{2} \tag{4}$$

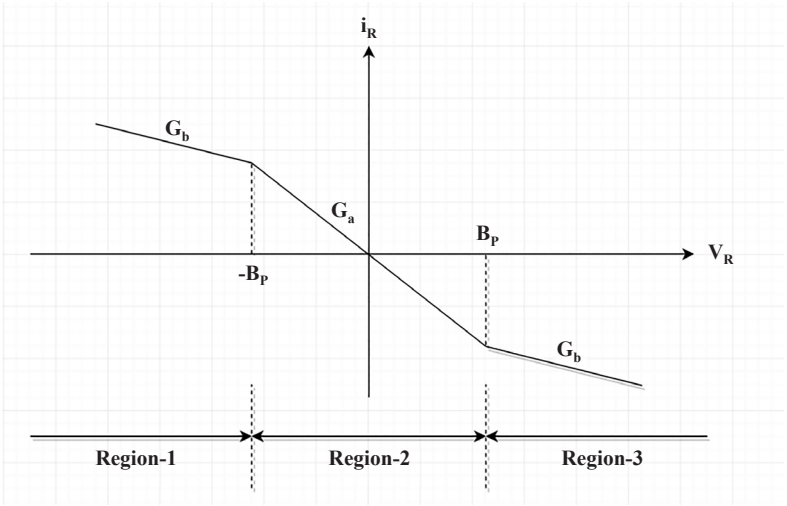

Figure 3. Current vs. voltage characteristics of Chua's diode graph

$$G_b V_R + (G_b - G_a) B_P \qquad V_R < -B_P \tag{5}$$

$$G_a V_R \qquad -B_P \le V_R \le B_P \tag{6}$$

$$G_b V_R + (G_a - G_b) B_P \qquad V_R > B_P \tag{7}$$

G_a and G_b are considered as the inner and outer slopes of Chua's diode, respectively, and $\pm B_P$ are the breakpoints in i_R (Figure 3).

Most of the analytical studies of the circuit will be focused on dimensionless form of the equations:

$$dx/dt = \alpha(y - x - f(x)) \tag{8}$$

$$dy/dt = x - y + z \tag{9}$$

$$dz/dt = -\beta y \tag{10}$$

Where $x = \frac{V_{C1}}{B_P}$, $y = \frac{V_{C2}}{B_P}$ and $z = (\frac{R}{B_P})$. i_L are dimensionless state variables and $\alpha = \frac{C_2}{C_1}$ and $\beta = \frac{R^2 C_2}{L}$ are the only two essential parameters. It is worth mentioning, that B_P has the same dimension as the voltage, the variables x, y and z are

dimensionless, as are the α and β parameters. Therefore, equations 8 to 10 hold from a dimensional analysis point of view.

2.3 Chaotic output

According to [33-37] Chua's circuit is the only known physical system which has been proven to have chaotic behavior in three different methods including computer simulations, laboratory experiments and mathematical analyses. The chaotic nature of the system comes from complex behavior that displays sensitive dependence on initial conditions. Several attempts have been made to understand Chua's circuit using different approaches such as investigating bifurcation phenomena and understanding nonlinear dynamic systems. By keeping all parameters in the above equations constant except for β, two periodic orbits are created simultaneously in a Hopf bifurcation (Figure 4). Then, by changing β they start to show a period-doubling cascade, as shown in Figure 4(c) and eventually the attractors begin to approach one another and reach chaos in Figure 4(f).

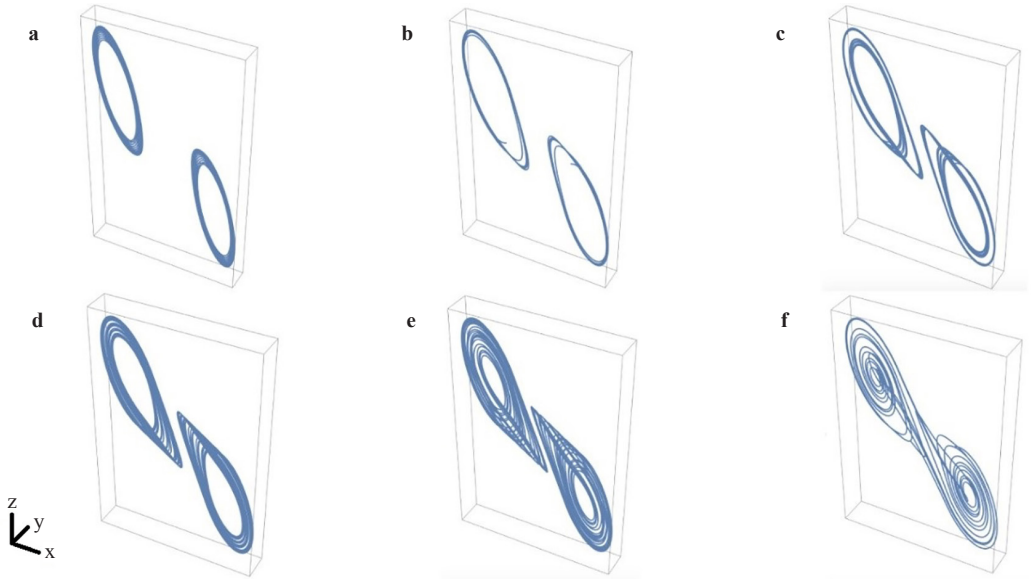

Figure 4. Fixed parameters are $\alpha = 10$, $G_a = \frac{8}{7}$, $G_b = \frac{5}{7}$. The attracting set starts to variate as parameter β changes. (a) $\beta = 25$, two periodic orbits. (b) $\beta = 20$, the orbits have "period-doubled". (c) $\beta = 18$, another doubling of the period. (d) $\beta = 17.8$, a pair of chaotic attracting orbits. (e) $\beta = 17.4$, the chaotic attractors expand and move toward one another. (f) $\beta = 15.4$, a "double scroll" chaotic attractor

3. Experimental setup

3.1 Chua's circuit

For resonating chaotic configurations like Chua's circuit, solid connections are required to observe accurate signals, therefore the classical configuration of Chua's circuit has been built on a custom-designed PCB (Printer Circuit Board) for experimental purposes. At one side of the 3 × 4 cm board the cupric connections are built, while the other side is covered with fiberglass as shown in Figure 5.

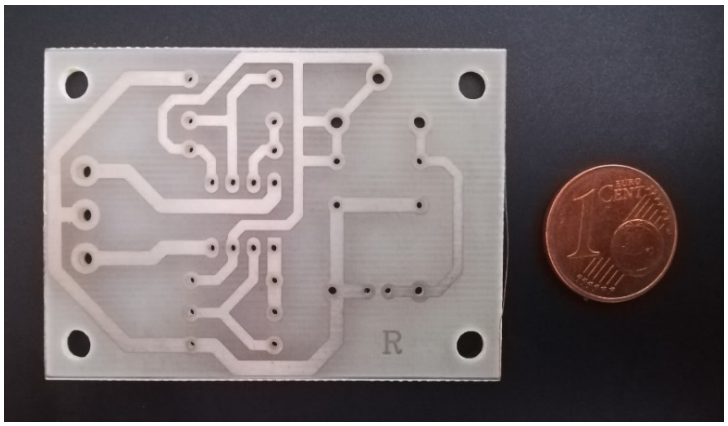

Figure 5. Custom designed PCB

Numerical simulations indicate that for the classical Chua's circuit of Figure 1 to exhibit chaotic behavior in the oscillation frequency, the components of the circuit should be set as indicated in Table 1. Whereas, the components' values presented in Table 2 could be used, had the Chua's diode been implemented using the configuration illustrated in Figure 2.

Table 1. parameters chosen for the experiment

Elements	Value
R	1.5 kΩ
R_1	220 Ω
R_2	220 Ω
R_3	2.2 kΩ
R_4	22.0 kΩ
R_5	22.0 kΩ
R_6	3.3 kΩ
C_1	10 nF
C_2	100 nF
L	15 mH

Table 2. Parameters chosen for alternative configuration of Chua's diode (Figure 2)

Elements	Value
R_7	290 Ω
R_8	290 Ω
R_9	1.2 kΩ
R_{10}	3.3 kΩ
R_{11}	3.3 kΩ
D_1	IN4148
D_2	IN4148

The final fabricated circuit is shown in Figure 6. The components were selected according to Table 1. The operational amplifiers are implemented using a TL082 PC Integrated Chip (IC), which includes two op-amps working with a supply voltage of 18 Volts provided by a battery. The inherent possible errors of the elements are listed in Table 3.

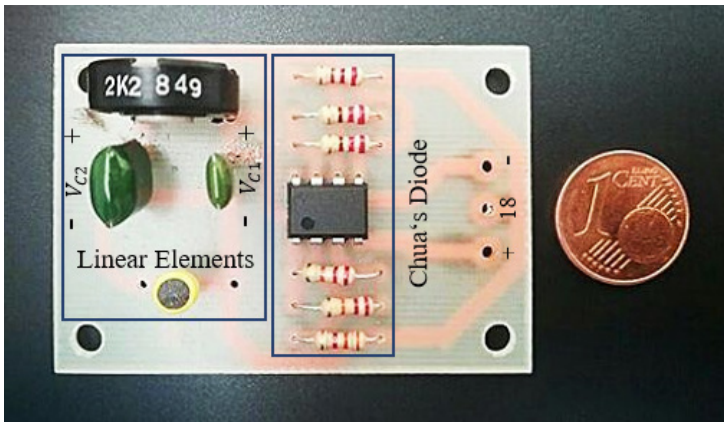

Figure 6. Chua's circuit

Table 3. Error percentage of circuit elements

Component	Error percentage
Resistance	5%
Capacitance	5%
Inductance	5%

The approach in the experiment is to plot the time-domain sampled version of the waveforms of V_{C_1} and V_{C_2}, where V_{C_1} and V_{C_2} denote the voltages of the capacitors C_1 and C_2, respectively.

3.2 Measurement devices

The chaotic signals obtained from Chua's circuit of Figure 6 are analog continuous time voltages in the range of around -33 V to +33 V. However, the mathematical schemes being used for the signal processing in the following sections of the manuscript are designed to be applied to discrete-time datasets. The Arduino microcontroller board presented in Figure 7 is used to perform the signal conversion from the analog domain to the required sampled values by means of the internal Analog to Digital Converter (ADC) block of the processor. The integrated ADC provides the equivalent voltage value representing the magnitude of the signal with continuous values for the sampled data.

In order to adapt the voltage levels of the Chua's circuit outputs, V_{C_1} and V_{C_2}, to a voltage level that is acceptable and processable by the microcontroller, a voltage amplifier as shown in Figure 8 is required. Using an LM324 Quad op-amp IC, which includes four operational amplifiers, the initial voltage level of V_{C_1} and V_{C_2} is transformed to 0-5 V. This process is done using two inverting amplifiers implemented by two op-amps with the gain less than one as defined by the ratio of R13 to R14 or equivalently R15 to R16, and an offset voltage generated by the remaining circuitries to shift the output voltage level to 0-5 V. It is worth mentioning that, for each sampled discrete-time input data, the Arduino is programmed to output the corresponding value of the capacitors' voltages in the range of -33 to 33.

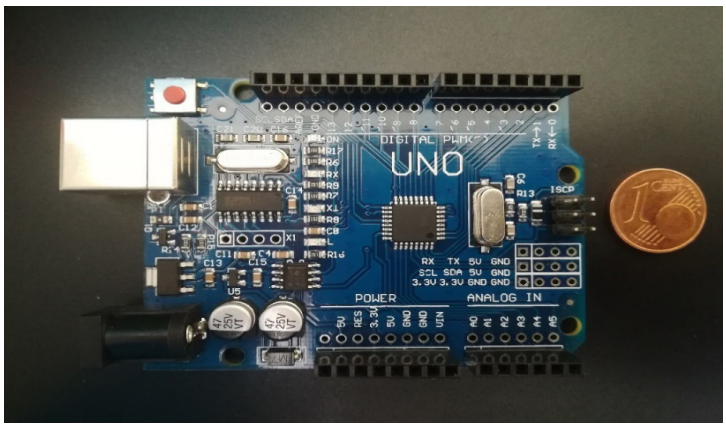

Figure 7. Arduino microcontroller

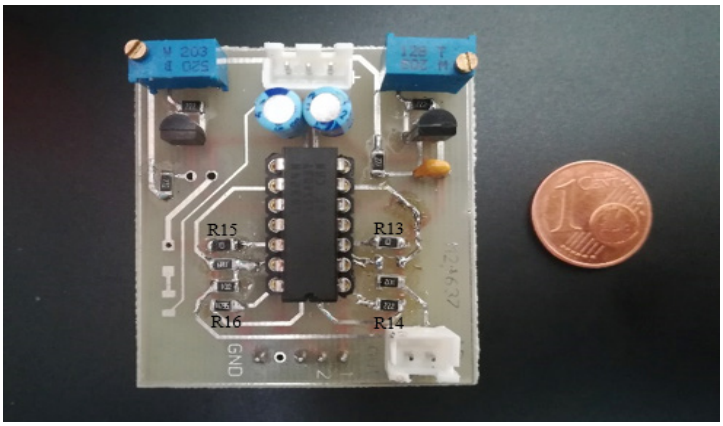

Figure 8. Voltage amplifier circuit

4. Methodology

4.1 Monte carlo algorithm-random inputs

For the sake of clarity in the concerns considered in the Monte Carlo Method as the main methodology of the current investigation, a brief explanation has been presented. Monte Carlo method is widely used for physical and mathematical problems, where a deterministic approach would be impossible to implement. The presented algorithm uses randomly generated values to produce numerical results to simulate the behavior of a system. Instead of considering all the influencing factors to formulate a general law, the method uses a rationally large and comprehensive set of randomized values and then this set is claimed to cover the whole domain of the problem. These algorithms can be applied to a vast range of problems, which have a probabilistic interpretation and are commonly used in a variety of fields such as optimization, numerical integration, generating samples from a probability distribution and simulating phenomena with significant uncertainty in inputs and numerous couple degrees of freedom. This makes the algorithm an appropriate technique when it comes to computational physics, many-body problems, weather forecasting, risk analysis and so on.

Monte Carlo integration is a method for approximately computing the value of complex integrals. Monte Carlo techniques are mostly used to provide numerical solutions for multi-dimensional functions, where they are too challenging to implement directly. The algorithm analyzes the results of possible inputs statistically; therefore, the current research is based on this method. Instead of having fixed inputs, Monte Carlo algorithms sweep the domain by adding random sets and evaluate the problem with that regard. Due to the necessity of well-controlled computational experiments in numerical methods such as the Monte Carlo algorithm[31], the experiment should be performed certain times to get better approximate outcomes.

4.2 Input data generation

Voltage alterations resulted from the implemented capacitors are considered as the output of the designed circuit. By applying them to the Monte Carlo integration after exerting the required manipulations, its level of randomness can be determined. For these manipulations, 8 schemes have been designed as mentioned below. The chaotic outputs of these schemes after being non-dimensionalized will be assigned to x and y pairs as the inputs of the Monte Carlo algorithm.

Each (x, y) represents a point on the Cartesian coordinate system. Both x and y should be in the range of [0, 1], therefore, the output of each scheme is divided by their maximum value. Bounded by the computational domain, the position of the dots should be limited to a unit square. Later, the number of points among them, which are also positioned inside a quarter of a circle will be calculated (Figure 9).

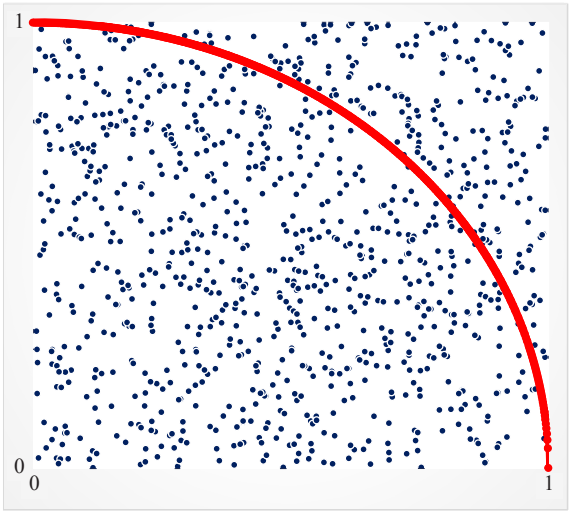

Figure 9. Computational domain

An adequate criterion to determine the level of randomness could be the extent of the proximity to the value of the quarter circle area, when the number of the points below the quarter circle curve in proportion to that of the entire data points is converging to $\pi/4$ as in Figure 10.

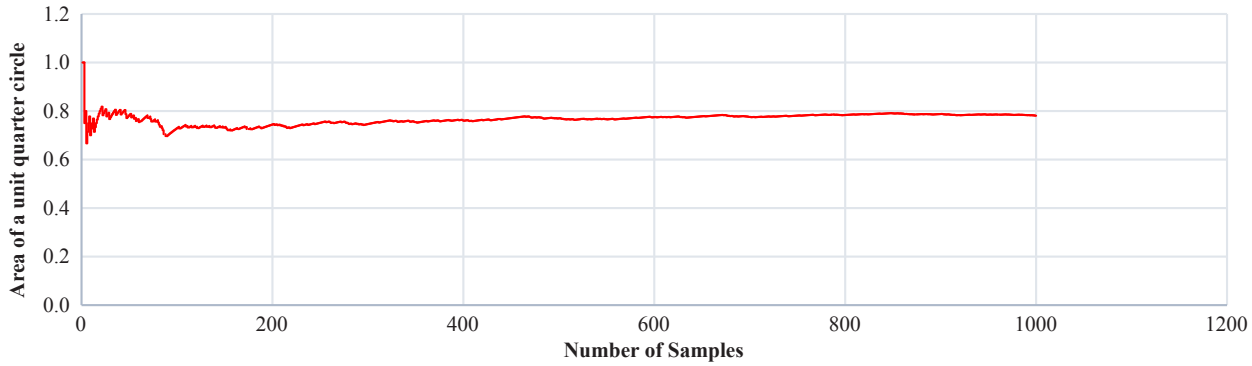

Figure 10. Convergence of Monte Carlo Integration Algorithm to $\pi/4$

4.2.1 Timer driven randomized data set

In the first scheme, instead of using voltage alteration resulted from the implemented capacitors as the output of the designed circuit, computer's timer driven randomized data set is used as to be inputted in the Monte Carlo algorithm; therefore, other scheme will be compared to the timer driven randomized data set to determine their level of randomness. Computer's algorithm for generating random numbers produces positive numbers smaller than 1, which are in the correct range for the Monte Carlo Integration according to what said before. These data sets will be non-dimensionalized by being divided to their maximum value, and after being simple-sampled over equidistant intervals of 4 ms will be inputted to the Monte Carlo integration.

$$Rand(t) = \{Random(t) | \forall\ t \in N\}$$

$$x = Rand(t) \qquad t \in N$$

$$y = Rand(t) \qquad t \in N \tag{11}$$

4.2.2 Simple sampling

In order to produce a scattering and chaotic set of data as to be inputted in the Monte Carlo algorithm, this scheme is simply designed to extract random samples from the raw measured dataset. For that matter, a particular set of data over

equidistant intervals of 4 ms have been selected, instead of a completely random selection and it is due to the chaotic nature of the signal voltages, which could be considered as entirely random in this case.

$$x = V_{11}(t) \qquad t \in N$$

$$y = V_{21}(t) \qquad t \in N \tag{12}$$

4.2.3 First time-derivative

In this scheme, the first-time numerical derivative of two followed data over equidistant intervals of 4 ms is the mathematical manipulation that produces a chaotic set of data exerted from the original dataset for the Monte Carlo Integration. However, this method produces outputs in the incorrect range according to the requirements of the Monte Carlo algorithm. Therefore, these outputs, after being mathematically transformed into the correct amplitude, will be assigned to the mentioned interval, and then used as the inputs of the Monte Carlo Integration.

$$x = \left| \frac{V_{11}(t_i) - V_{11}(t_{i-1})}{t_i - t_{i-1}} \right| \qquad t \in N$$

$$y = \left| \frac{V_{21}(t_i) - V_{21}(t_{i-1})}{t_i - t_{i-1}} \right| \qquad t \in N \tag{13}$$

4.2.4 Root of squared time derivatives

In this scheme the way of producing chaotic and scattering data is similar to the previous section. The first time-derivative of two consecutive data over equidistant intervals of 4 ms is calculated. As mentioned before, this method produces outputs in the inadequate range of [-1, 1]. So, in order to transfer the outputs into the correct range of [0, 1] in this section, the root of the squared time derivative is calculated. In the end, a new set of data has been exerted from the last set of outputs will be used as the required inputs of the Monte Carlo Integration.

$$x = \sqrt{\left(\frac{V_{11}(t_i) - V_{11}(t_{i-1})}{t_i - t_{i-1}}\right)^2} \qquad t \in N$$

$$y = \sqrt{\left(\frac{V_{21}(t_i) - V_{21}(t_{i-1})}{t_i - t_{i-1}}\right)^2} \qquad t \in N \tag{14}$$

4.2.5 Frequency indicator

In order to obtain an indicator of the longitudinal behavior of the original signal, this scheme addresses the instantaneous frequency opposing to the common consideration of the amplitude as the scattering and chaotic data set derived from continuous-time signal. However, a mean frequency indicator over equidistant intervals has been considered, instead of a more usual instantaneous frequency, since the further requirements of the Monte Carlo algorithm demand one to switch to a digital sampling of the data anyway. For that matter, the measured data has been cut to intervals of 4 ms. Then, the number of alterations in the algebraic sign of the first time derivative in each interval has been assigned to the said interval, and then used as the mathematically manipulated data set inputted to the Monte Carlo Integration method.

$$x = \sum_{t_i}^{t_{i+T}} U(-(V_{11}'(t_i^-) * V_{11}'(t_i^+))) \qquad t \in N$$

$$y = \sum_{t_i}^{t_{i+T}} U(-(V_{21}'(t_i^-) * V_{21}'(t_i^+))) \qquad t \in N \tag{15}$$

4.2.6 Time interval between two consecutive extremums (Time extremum distance)

This scheme addresses the time interval between two consecutive extremums as a factor of producing chaotic and scattering data set exerted from the raw signals for the Monte Carlo Integration. The extremums are found with numerical

derivation of the data and checking sign alterations to find whether the investigated point could be considered as an extremum. At last, by subtracting the time established to every two consecutive extremums, the input of the Monte Carlo integration would be ready.

$$x = t_i - t_{i\text{-}1} \quad if\ (V_{11}(t_i) = extremum\ and\ V_{11}(t_{i\text{-}1}) = extremum)$$

$$y = t_i - t_{i\text{-}1} \quad if\ (V_{21}(t_i) = extremum\ and\ V_{21}(t_{i\text{-}1}) = extremum) \tag{16}$$

4.2.7 Voltage interval between two consecutive extremums (Y extremum distance)

With regard to demonstrating the voltage alteration between each two following extremums of the signal, the current method would be considered as the next schematic. The algorithm of finding the extremums is as mentioned above with a difference in the established value, which is the voltage of the extremum and it should be mentioned that the subtraction of the consecutive extremums can cause the result value to have different signs. Therefore, similar to the other schemes, a shift would be applied to the data to fit in the [0, 1] range.

$$x = V_1(t_i) - V_1(t_{i\text{-}1}) \quad if\ (V_{11}(t_i) = extremum\ and\ V_{11}(t_{i\text{-}1}) = extremum)$$

$$y = V_2(t_i) - V_2(t_{i\text{-}1}) \quad if\ (V_{21}(t_i) = extremum\ and\ V_{21}(t_{i\text{-}1}) = extremum) \tag{17}$$

4.2.8 Riemann integration method

This scheme measures the effect of integration on producing chaotic and scattering data sets as the requirements of the Monte Carlo integration. In order not to get involved with the complex mathematical calculations, Riemann integration is used on the input data, since it is the simplest integration algorithm. Riemann integration approximates the area under a curve by breaking up the said area into rectangles and calculating the sum of areas of those rectangles. Therefore, the measured signal is cut into intervals of 4 ms. Then, to each interval the multiplication of the average of the two following voltages of the measured signal and the time interval between them will be assigned as the Riemann integration of that interval. The sum of Riemann integration of 4 ms consecutive intervals after being simple-sampled will be the required chaotic and scattering inputs for the Monte Carlo Integration.

$$x = \sum_{t_i}^{t_{i+T}} \frac{(V_{11}(t_i) + V_{11}(t_{i-1}))/2}{t_i - t_{i-1}} \qquad t \in N$$

$$y = \sum_{t_i}^{t_{i+T}} \frac{(V_{21}(t_i) + V_{21}(t_{i-1}))/2}{t_i - t_{i-1}} \qquad t \in N \tag{18}$$

4.2.9 Natural logarithm of consecutive experiments

In this scheme the natural logarithm of subtraction of two signals extracted from consecutive experiments is the mathematical manipulation which produces the scattering and chaotic data as the inputs of the Monte Carlo integration. As mentioned above, for this section two consecutive experiments would be executed, and due to the lack of sensitivity and errors of the implemented elements, the results would be different as it resembles the nature of chaos. The measured data will be cut into several intervals of 4 ms. Then natural logarithm of the absolute value of the subtraction of the voltages of the two signals with exact time will be calculated. After these manipulations, a new data set will be simple sampled which will become the chaotic and scattering inputs required for the Monte Carlo Integration.

$$x = Ln(|V_{11}(t_i) - V_{12}(t_i)|) \qquad t \in N$$

$$y = Ln(|V_{21}(t_i) - V_{22}(t_i)|) \qquad t \in N \tag{19}$$

5. Results and discussion

As the primary objective of the current research a quantitative comparison between 9 mathematical schemes/functions driven based on the output voltage signals measured over the capacitors of a classic Chua's circuit is established. In order

to have a set of criteria quantifying, while evaluating, the level of randomness of the resulting mathematically manipulated data, a geometric manifestation of the Monte Carlo Integration algorithm has been utilized, in which a quarter circle of unit radius has been swept by points of normalized coordinates, each obtained from one of the above mentioned voltages undergoing a mathematical scheme, as discussed in the previous section. The final evaluation has then been carried out by checking the ratio of the fraction of swept area to that of the entire quarter circle, which would estimate a numerical value for the constant π, should this sweeping occur uniformly throughout the computational domain.

The results of the scattering data in the Monte Carlo algorithm in one view have made an opportunity to make them comparable. As a matter of clarification, it should be mentioned that to cover all the data including both positive and negative voltages for some schemes (*Simple sampling* (*b*)-*First time derivative* (*c*)-*Voltage interval between two consecutive extremums* (*g*)-*Riemann integration method* (*h*)), a shifting transform was applied to the manipulated data in order to make it accessible for the Monte Carlo algorithm; so as if the stated process was taken, it can be concluded that the data which are located in the center, top and bottom of the graphs in Figure 12 are valued nearly zero, positive and negative, respectively.

Simple sampling shows a wide distribution of data over the domain as can be seen in Figure 12 (b). Also, because of the physical limitations of the experiment some values can never be accepted by the capacitors, which have been left blank on the mentioned graph.

In *First time-derivative*, *Root of squared time derivative* and *Riemann integration methods*, the derivation and the integration of the voltage graph with a reasonable shift, to be in a specific range is demonstrated. As shown in Figure 12 (c), there is a dense distribution of data in the central part of the domain resulted from the numerous oscillations in the chaotic signal (Figure 11), that could lead to having many extremums as well, and it means that the first-time derivatives are zero so they would be displayed in the center. The next scheme (Figure 12 (d)) is similar to the previous one with a small difference in its area transformation. The operation of root of square time derivatives makes the plot look similar to the top right of the Figure 12 (c). The behavior of the *Riemann integration scheme* states that in a specific time range, a numerical integration, in which the upper parts of the signal considered positive and the lower parts considered negative (Figure 11), should be applied and because of the chaotic nature of the signal, which causes consecutive oscillations, the summation of the calculated areas would be mostly zero. Therefore, the condensed central distribution of data in Figure 12 (h) could be explained.

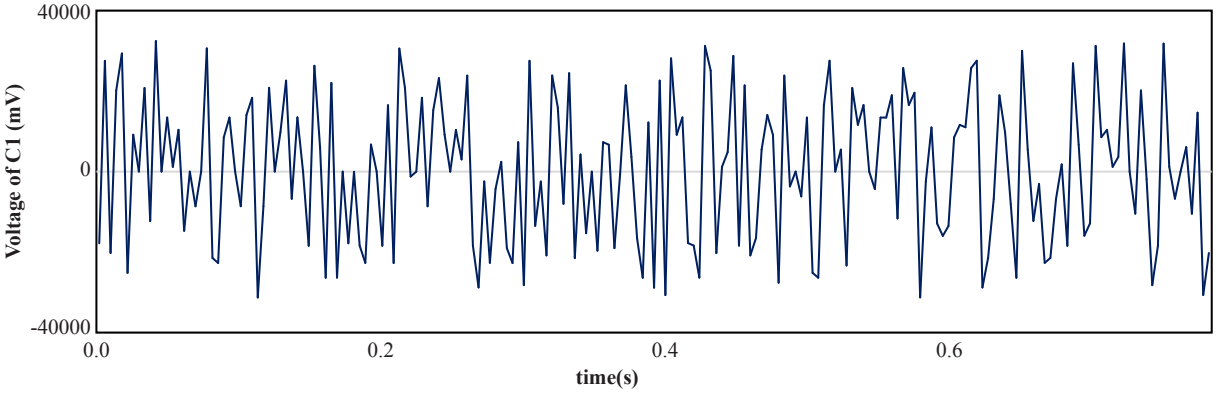

Figure 11. Output signal of Capacitor 1

It is assumable from the mathematical behavior of the time-domain waveform of the voltage for both capacitors that each maximum extremum can only be followed by a minimum one and the same goes for the opposite situation. As a result of the stated fact, the outputs sign changes once in a row; therefore, there exist only two possibilities when mapping the outputs of the two capacitors. Either values with equal signs or values with opposite signs could be mapped. The occurrence of both situations depends on whether the initial slope of the mentioned graph for both capacitors have the same sign or not (Figure 12 (g)). In the current paper, values with the same signs have been mapped. Due to the shift in the domain, in order to plot the results in the correct range for the sake of comparison, the graph displays two squares in the Cartesian coordinates.

Since the number of alterations of the signal's scope in a particular time changes between some specific quantities (Figure 11), due to choosing a limited interval time, the below-demonstrated results of the *frequency indicator* scheme were expected to behave discretely. But, if the data set number was allowed to reach a large quantity, in consequence of

the unlimited data, the area of the square would have been covered completely. Again, in *time interval* scheme, due to the chaotic behavior of the output signal and the certain rate of sampling of the experiment (i.e. 4 ms), the discrete form of the distribution could be described by the philosophy of the algorithm, since every extremum in the time axis is a multiple of 4 ms.

An explanation for the form of dense distribution of the data in the top right of *natural logarithm* scheme could be the nature of exponential behavior of the *ln function.* That is due to the fact that, in small quantities, because of the low slope of the function, the differences in the input values would not change the outcome intensively, and the exact opposite description applies to the rest of the graph of *natural logarithm* of consecutive experiments. This means, the higher the given inputs, the greater the change in the final result will be, and as long as a limited accuracy in sampling of the voltages exists, the subtraction of the two voltages could not obtain a certain amount to sweep all the domain, hence the uncovered area displayed in Figure 12 (i).

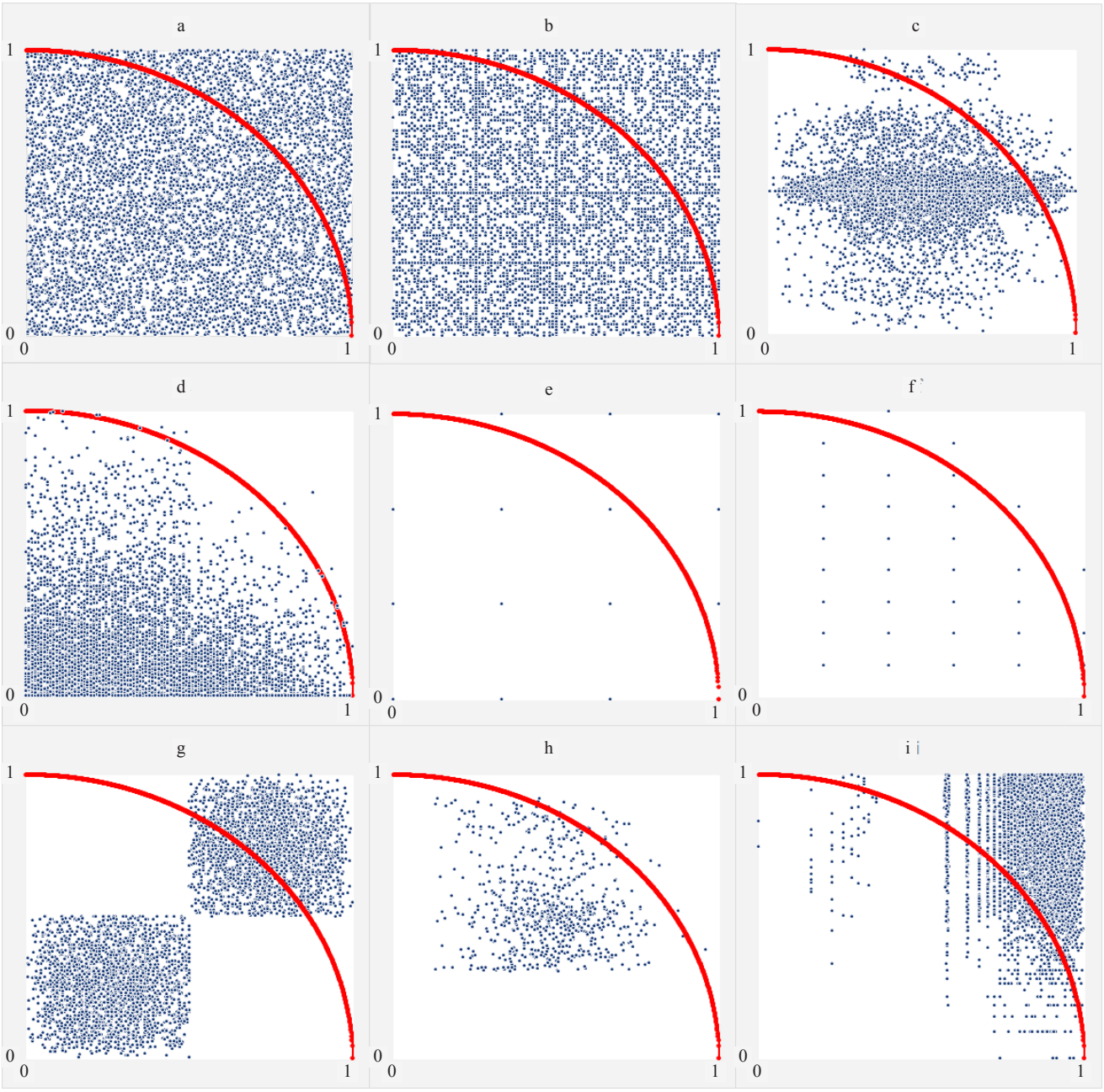

Figure 12. Results of the scattering data in the Monte Carlo algorithm. Horizontal axis: voltage of C1, Vertical axis: voltage of C2-a) Timer driven, b) Simple sampling, c) First time derivative, d) Root of squared time derivatives, e) Frequency indicator, f) Time interval between two consecutive extremums, g) Voltage interval between two consecutive extremums, h) Riemann integration method, i) Natural logarithm of consecutive experiments

Table 4. Convergence results

Mathematical Scheme	Data Set Number	Convergence Rate	Convergence Margine	Calculated Pi Number	Deviation From Pi	Deviation percentage
Frequency Indicator	2500	2300	0.0003	3.1424	0.0009	0.02%
Randomized-timer	7500	5258	0.0003	3.1304	-0.0101	-0.32%
Simple Sampling	7500	5441	0.0003	3.2576	0.1161	3.69%
Y Extremum Distance	4950	4407	0.0003	2.6604	-0.4811	-15.31%
Integration	750	672	0.0150	3.8668	0.7253	23.08%
F´(x)	7500	2570	0.0003	3.9428	0.8013	25.50%
SQRT(F´^2)	7500	450	0.0003	3.9904	0.8489	27.02%
Time Extremum Distance	3750	2716	0.0003	3.9916	0.8501	27.06%
Natural logarithm (ln)	7025	3600	0.0003	0.4632	2.6783	85.25%

Table 4 summarizes the final results of the investigated schemes to find the accuracy of each one in estimating the Pi number by manipulating a truly set of chaotic data to make a random one. The experiment has been performed only once and according to the explanation, the voltage of the capacitors in every 4 ms have been used as the raw input, which results in all the schemes having identical inputs. However, because of the mathematical manipulation applied to each scheme, the amount of the data used as the input of the Monte Carlo algorithm in each scheme may differ from others. Therefore, the first column of this table has been dedicated to manifest the amount of data, which has been used for the Monte Carlo algorithm in each scheme.

In order to find the span of the set of data, in which the calculated Pi number for each scheme converges to the final calculated value, a criterion has been assessed according to the corresponding graphs (Figure 13). For that, the subtraction of Monte Carlo algorithm output for two consecutive data has been divided by the maximum value of this subtraction, then in each scheme these ratios have been compared to a pre-defined threshold, presented on the third column of the table. The n-th data, from which all the ratios have smaller values than the threshold, has been chosen as the convergence rate of that scheme, and it is shown in the second column of Table 4.

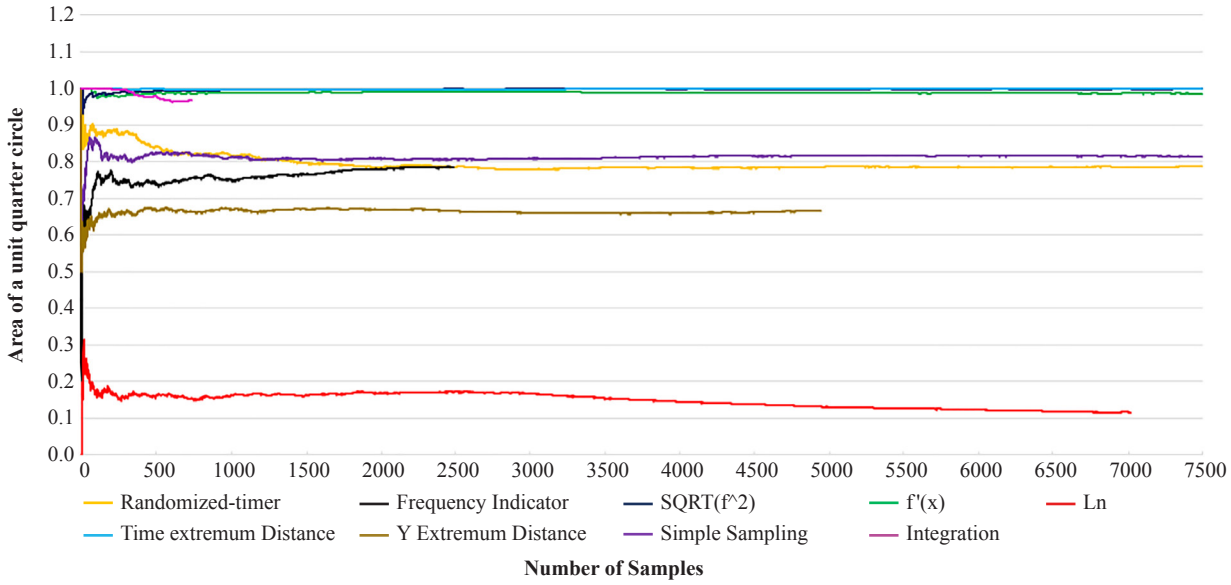

Figure 13. Convergence chart of the schemes to the quarter of calculated Pi value

All the thresholds have been fixed on 0.0003, except for the *integration* scheme. In this scheme, as Figure 12 (h) displays, the center of the graph has a condense distribution of data, which makes the subtraction of the output for each data, and the maximum value of this subtraction adjacent. Therefore, these ratios cannot possess values less than a specific number. This characteristic of the mentioned scheme makes an obligation to choose a special threshold, that compensates for this feature.

Two extra columns have been added into the above table as a matter of comparing the final results of the current research with the analytical Pi number. The comparisons have been made in two ways. First, the deviation of the estimated Pi from its actual value has been shown in column 5 of the table, for each scheme. And then, the ratio of these subtractions to the analytical Pi forms the last column. It is to be witnessed, that the negative and positive deviations represent under-, and over-estimations of the analytical value, respectively. This rule applies to both columns.

Although the main philosophy of *Y extremum distance* and *time extremum distance* is to determine the localized maximums and minimums of the chaotic signal in the voltage and the time axes, respectively, there exists a considerable difference between the final outcomes of the Pi estimation in the studied schemes. Due to the constant rate of sampling, the *time extremum distance,* with its calculation process being described before in 4.2.6, would be obliged to show results in just limited calculated multiples of the sampling rate (4 ms), and consequently would not cover all the area but in the *Y extremum* scheme, no such limitation has appeared and the chaotic nature of the resulting data set would itself act as a trigger to the random sweeping of the domain.

A misconception may exist, where there is a difference between the estimated Pi in *Y extremum distance* and *simple sampling* schemes, while both are dealing with the original chaotic data. To resolve this issue, one should consider that the algorithm of *Y extremum distance* scheme operates a mathematical variation, which leads to the fact that the sign of each individual output would be the reverse of the previous one, thus by asserting the above conditions for both of the voltages, only two quarters of the computational domain would be swept by the data depending on the initial slope of the graph. But the *simple sampling* scheme deals with the original non-manipulated data, which could cover the entire domain. Therefore, a better estimation was expected for the latter scheme.

A significant difference between the convergence rate of $F'(x)$ and $SQRT(F'^2)$ is observed, despite the two being derived from a quite similar algorithm. Due to the limited range of the $SQRT(F'^2)$ scheme, it can be assumed that each point in the $F'(x)$ scheme with any specific coordinates would be transferred to the top right of the computational domain, where all the data is positive (Figure 12 (c)), hence the only essential parameter for the random positioning of the points would be the distance of each point to the center of the domain. Having the $F'(x)$ scheme domain divided into four separate parts, it would result in the $SQRT(F'^2)$ scheme with a convergence rate being four times smaller.

However, as the lowest ranked scheme; i.e. *Natural Logarithm*, the result sets plotted in the computational domain correspond to less scattered and normally distributed points. The numerical value of Pi calculated from this scheme shows less satisfactory randomly sweeping of the domain. The reason could be addressed in regard to the mathematical nature of the *ln* operator; as it tends to compress numerical values in their orders of magnitude with respect to the constant Euler Number (Napier's Constant)'. This process of reduction will generate well distributed results for the input signals with great changes in amplitude, however, as could be seen in the experimental measurements of the Chua's circuit, which was the basis of the computations in the current research, the proximity of the data in a rather narrow vicinity has led to less randomly distributed fashion of the (x, y) pairs in the domain, and consequently a prediction of the value Pi with an undesirable precision.

As shown above, the *frequency indicator* is the most exact approximation and has the least distance from Pi amongst the other schemes. Next, the acceptable applied schemes are the *Y extremum distance* and the *simple sampling* algorithm. *Frequency indicator* has a discrete distribution of data as shown in Figure 12 (e). This makes the exact estimation of Pi in this scheme a counter-intuitive one. Also, the symmetrical system of dispensation causes the output to depend on the number of the recurrence of each specific input, but not exactly on its position, and the scattering distribution of the points. This scheme shows a high repetition of data in the center and a low distribution on the edges of the domain; therefore, its specific results could be explained by a Gaussian distribution.

Having the computational domain divided by smaller but not quite infinitesimal sections, i.e. one third of the unit length, 9 squares (Figure 14) will be constructed. Each point in Figure 12 (e) represents a corresponding point among the set of points inside a square, the distribution function of which is the Gaussian function (Figure 15).

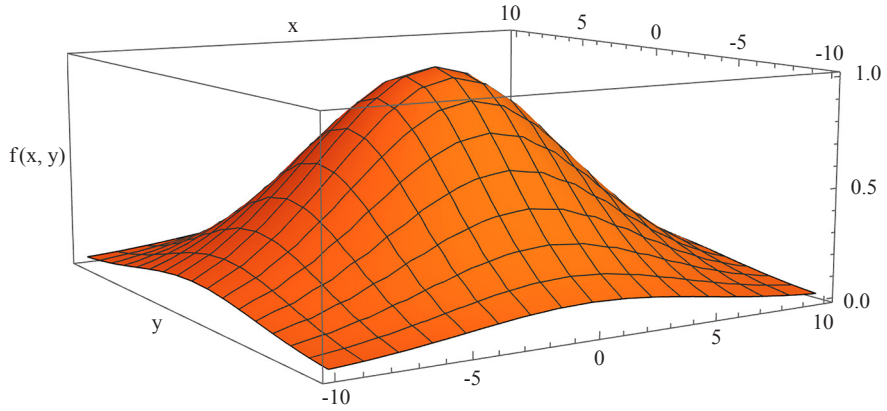

Figure 14. Gaussian distribution in frequency indicator scheme

$$f(x,y) = Exp\left[-\left(\frac{x^2}{2a^2}+\frac{y^2}{2a^2}\right)\right] \tag{20}$$

where, $a = 2.058$, x and y represent the horizontal and vertical axes, respectively, the origin being chosen at a point, where probability of occurrence is at its highest, and the range for x and y being defined from -10 to 10.

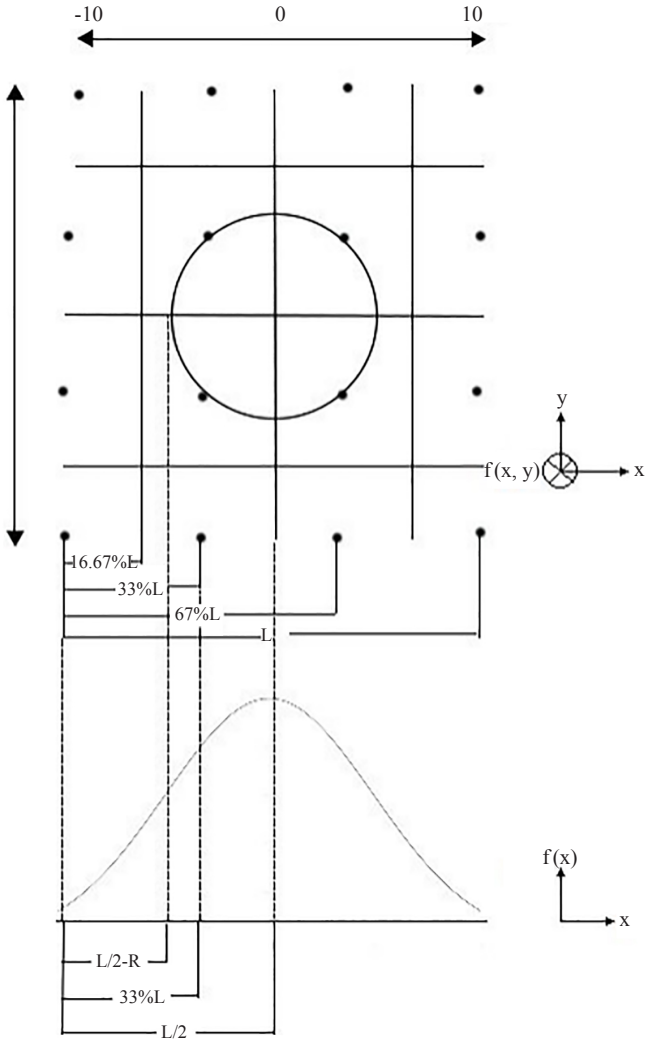

Figure 15. Simplified recurrence distribution of the frequency indicator scheme

Pi is calculated using the equation below.

$$\frac{\pi}{4} = \frac{4 \times P_4 + 7 \times P_7}{4 \times P_4 + 12 \times P_7} \tag{21}$$

where P_4 and P_7 are the probabilities of occurrence in the four central squares, and in the peripheral ones, respectively.

$$R = L\sqrt{\frac{16.67^2}{100} + \frac{16.67^2}{100}} \tag{22}$$

Finally, benefitting from the symmetry of the problem, all the calculations at this point have been taken place in the $y = 0$ plane, while not imposing any change to the general premises of the problem. In these calculations, P_4 is the ratio of the number of points located in the central section to the number of points located in the ± 16% range of the x axis, and P_7 is the ratio of the number of points located in the ± 33% range of the x axis to the number of points located in the ± 41% range of the x axis.

$$P_4 = \frac{f(0,0)}{f(2.3,0)} \tag{23}$$

$$P_7 = \frac{f(3.3,0)}{f(5,0)} \tag{24}$$

In conclusion, this Gaussian distribution indicates that the data in the *frequency indicator* scheme (Figure 12 (e)), act similarly, and estimate Pi nearly accurately.

After investigating all the mentioned schemes, comparing the final results of the Monte Carlo as in Figure 13, which demonstrates the estimation of the Pi value and gives a clear view on where the convergence of each scheme starts from, is the last item in the results and discussion section. According to Figure 13, *frequency indicator* and *simple sampling* schemes have the best estimation of Pi value among all the schemes, which means the number of extremums over equal time intervals of voltage-time graph of the Chua's circuit capacitors and the voltage values themselves were the best algorithms aligned with the purpose of this study than the other generated methods. However, there exist some schemes such as *Natural logarithm, Riemann integration method, Time extremum distance and SQRT(F'^2),* which do not provide acceptable approximations for Pi.

6. Conclusion

The main aim of the manuscript is to evaluate the randomness level of 8 defined schemes, which are mathematically manipulated sets of experimental driven chaotic data produced by a classical configuration of Chua's circuit by using the Monte Carlo Integration algorithm. Therefore, it can be concluded that the result of this research has an application in the realm of Random Number Generators (RNGs). In the first steps of the work, a chaotic signal was generated from the Chua's circuit after finding the chaos-producing range of the resistors. The experimental data were then inserted into 8 different mathematical manipulation schemes and lastly, the results were utilized as the inputs of a geometrical manifestation of the Monte Carlo Integration algorithm.

In order to make the output of the current research comparable to the existing methods of generating random sets of data, a scheme was designed to only use the computer random number generation method for estimating of Pi by the help of the Monte Carlo algorithm. This scheme has been used as an evaluator in this research. All the eight remaining schemes will be compared to the first one. Whether or not these estimations are closer to Pi is this paper's criterion of choosing the scheme producing the most scattering and chaotic sets of random numbers.

By considering the explained scheme as the evaluator on this research, all the 8 schemes have been ranked according to the fulfillment of the above-mentioned criterion. Applying this logic has resulted in the *frequency indicator* scheme having the closest approximation of 3.1424 for Pi, and the *natural logarithm* scheme with the estimated value of 0.4632 for Pi, being the most diverged one. *Frequency indicator* scheme shows the best estimation of Pi value among all, which means the number of extremums over equal time intervals of voltage-time graph of the Chua's circuit capacitors produces most satisfying results than the conventional method of timer driven random number generating.

References

[1] Kevin M. Cuomo, Alan V. Oppenheim. Circuit implementation of synchronized chaos with applications to communications. *Physical Review Letters*. 1993; 71: 1.

[2] W. Kinzel, A. Englert, I. Kanter. On chaos synchronization and secure communication. *Phil. Trans. R. Soc. A*. 2010; 368: 379-389.

[3] Lorenz, Edward N. Deterministic Nonperidic Flow. *Journal of the Atmospheric Sciences*. 1963; 20(2): 130-141.

[4] Louis M. Pecora, Thomas L. Carroll. Synchronization in Chaotic Systems. *Physical Review Letters*. 1990; 64(8): 821-825.

[5] S. Boccaletti, C. Grebogi, Y. C. Lai, H. Mancini, D. Maza. The control of chaos: theory and application. *Physics Reports*. 2000; 329: 103-197.

[6] Charlotte Werndl. What are the new implications of chaos for unpredictability? *The British Journal for the Philosophy of Science*. 2009; 60(1): 195-220.

[7] Hongbin Zhang, Chunguang Li, Jian Zhang, Xiaofeng Liao, Juebang Yu. Controlling chaotic Chua's circuit based on piecewise quadratic Lyapunov functions method. *Chaos, Solitons & Fractals*. 2004; 22(5): 1053-1061.

[8] Shihua Li, Xiangze Lin, Yu-Ping Tian. Set stabilization of Chua's circuit via piece-wise linear feedbacks. *Chaos, Solitons & Fractals*. 2005; 26(2): 571-579.

[9] C. Cruz-Hernández, N. Romero-Haros. Communicating via synchronized time-delay Chua's circuits. *Communications in Nonlinear Science and Numerical Simulation*. 2008; 13(3): 645-659.

[10] Badr Saad T. Alkahtani. Chua's circuit model with Atangana-Baleanu derivative with fractional order. *Chaos, Solitons & Fractals*. 2016; 89: 547-551.

[11] Cherif Aissi, Demetrios Kazakos. A Review of Chaotic circuits, Simulation and Implementation. *Proceedings of the 10th WSEAS International Conference on CIRCUITS*. 2006. p.125-131.

[12] S. Di Gennaro, F. Di Paolo. Output tracking for Chua's circuit in presence of disturbances. *IFAC Proceedings Volumes*. 2005; 38(1): 276-281.

[13] Chun-Ni Wang, Jun Ma, Yong Liu, Long Huang. Chaos control, spiral wave formation, and the emergence of spatiotemporal chaos in networked Chua circuits. *Nonlinear Dynamics*. 2012; 67: 139-146.

[14] K. Murali, Haiyang Yu, V. Varadan, H. Leung. Secure communication using a chaos-based signal encryption scheme. *IEEE Transactions on Consumer Electronics*. 2001; 47(4): 709-714.

[15] K. Cuomo, A. Oppenheim, S. Strogatz. Synchronization of Lorenz-based chaotic circuits with applications to communications. *IEEE TCAS II: Express Briefs*. 1993; 40: 626-633.

[16] R. Lozi. Designing Chaotic Mathematical Circuits for Solving Practical Problems. *Int. J. Automation and Computing*. 2014; 11: 588-597.

[17] G. Gharooni-fard, F. Moein-darbari. A New Approach to Network Optimization Using Chaos-Genetic Algorithm. *Computational Optimization and Applications in Engineering and Industry*. Springer; 2011. p.245-270.

[18] Golnar Gharooni-fard, Fahime Moein-darbari, Hossein Deldari, Anahita Morvaridi. Scheduling of scientific workflows using a chaos-genetic algorithm. *Procedia Computer Science*. 2012; 1(1): 1445-1454.

[19] Matej Šalamon. Chaotic Electronic Circuits in Cryptography. In: Dr. Jaydip Sen. (ed.) *Applied Cryptography and Network Security*. 2012.

[20] Hector Puebla, Jose Alvarez-Ramirez, Ilse Cervantes. A Simple Tracking Control for Chua's Circuit. *IEEE Transactions on Circuits and Systems-I: Fundamental Theory and Applications*. 2003; 50(2).

[21] Cruz-Hernández C, Nijmeijer H. Synchronization through filtering. *International Journal of Bifurcation and Chaos*. 2000; 10(4): 763-75.

[22] Sira-Ramírez H, Cruz-Hernández C. Synchronization of chaotic systems: A Generalized Hamiltonian systems approach. *International Journal of Bifurcation and Chaos*. 2000; 2(5): 769-773.

[23] López-Mancilla D, Cruz-Hernández C. Output synchronization of chaotic systems: Model-matching approach with application to secure communication. *International Journal of Nonlinear Dynamics and Systems Theory*. 2005; 5(2): 141-156.

[24] Feldmann U, Hasler M, Schwarz W. Communication by chaotic signals: the inverse system approach. *International Journal of Circuit Theory and Applications*. 1996; 24: 551-579.

[25] Jose M. Cruz, Leon O. Chua. A CMOS IC Nonlinear Resistor for Chua's Circuit. *IEEE Transactions on Circuits and Systems-I: Fundamental Theory and Applications*. 1992; 39(12).

[26] Michael Peter Kennedy. Three Steps to Chaos-Part 2: A Chua's Circuit Primer. *IEEE Transactions on Circuits and Systems-I: Fundamental Theory and Applications*. 1993; 40(10).

[27] Leon O. Chua. Chua's circuit: an overview ten years later. *Journal of Circuits, Systems and Computers*. 1994; 4(2): 117-159.

[28] Holokx A. Albuquerque, Rero M. Rubinger, Paulo C. Rech. Theoretical and experimental time series analysis of an inductorless Chua's circuit. *Physical Review D*. 2007; 233: 66-72.
[29] Jessica R. Piper, J. C. Sprott. Simple Autonomous Chaotic Circuits. *IEEE Transactions on Circuits and Systems-II: Express Briefs*. 2010; 57(9): 730-734.
[30] J. C. Sprott. A new class of chaotic circuit. *Physics Letters A*. 2000; 266: 19-23.
[31] Caflisch, R. E. *Monte Carlo and quasi-Monte Carlo methods*. Cambridge University Press; 1998. p.1-49.
[32] T. Matsumoto. A chaotic attractor from Chua's circuit. *IEEE Transactions on Circuits and Systems*. 1984; 31(12): 1055-1058.
[33] Leon O. Chua, Ljupco Kocarev, Kevin Eckert. Experimental Chaos Synchronization in Chua's Circuit. *International Journal of Bifurcation and Chaos*. 1992; 2(3): 705-708.
[34] L. Fortuna, M. Frasca, M. G. Xibilia. *Chua's Circuit Implementation: Yesterday, Today and Tomorrow*. Singapore: World Scientific; 2009.
[35] Prem Bhushan Mital, Umesh Kumar, Rai Sachindra. Chua's Circuit-A Universal Paradigm for Generating and Studying Chaos. *Journal of Active and Passive Electronic Devices*. 2008; 3: 51-63.
[36] Kathleen T. Alligood, Tim D. Sauer, James A. yorke. *Chaos: An Introduction to Dynamical Systems*. Textbooks in Mathematical Sciences. Springer-Verlag New York Inc; 1996.
[37] T Matsumoto, Leon O Chua, M komuro. The double scroll bifurcations. *Circuit Theory and Applications.* 1986; 4: 117-146.